Rotational Spectra of Phosphorus Monosulfide up to 1 THz

H. Klein, E. Klisch, and G. Winnewisser

Universität zu Köln, Zülpicher Str. 77, D-50939 Köln

Z. Naturforsch. **54 a,** 137–145 (1999); received November 21, 1998

The submillimeter-wave rotational spectrum of the PS radical in the electronic and vibrational ground state ($X^2\Pi_{1/2}$, $X^2\Pi_{3/2}$) was recorded with the Cologne terahertz spectrometer in the frequency region between 540 GHz and 1.07 THz, covering rotational quantum numbers from $J = 30.5$ to 60.5. The PS radical has been produced by discharging $PSCl_3$ buffered with Ar. For all transitions the Λ-doubling was resolved for both the $^2\Pi_{1/2}$ and $^2\Pi_{3/2}$ states. For some transitions with $\Delta F = 0$ the hyperfine structure (hfs) caused by the P-atom could partially be resolved even for rather high J values. Analysis of the complete rotational data set of PS allows the derivation of a full set of molecular parameters, including the rotational constants B, D, H, the fine-structure constants A, γ, D_γ, the parameters for the Λ-doubling p, D_p, q, and the magnetic hyperfine constants a, b, c, d, C_I. All parameters have been determined, whereby a, c, and the nuclear spin rotation-constant C_I were obtained for the first time.

I. Introduction

In the laboratory the PS radical was first studied by Dressler in 1955, who investigated part of the electronic spectrum and assigned the measured spectra arising from the $C^2\Sigma - X^2\Pi$ and $B^2\Pi - X^2\Pi$ band systems in the wavelength regions between 2700 - 3100 and 4200 - 6000 Å respectively [1].

The fundamental vibrational band of PS near 733 cm^{-1} was measured by Kawaguchi et al. (1988), using a diode laser spectrometer [2]. The rotational structure of this fundamental band was clearly resolved for the $^2\Pi_{1/2}$ and $^2\Pi_{3/2}$ states and assigned in agreement with the rotational constants and the value for the fine structure parameter ($A = 321.93$ cm^{-1}) given by Jenouvrier and Pascat [3]. They carried out a rotational analysis of the two band systems $C^2\Sigma - X^2\Pi$ and $B^2\Pi - X^2\Pi$.

Simultaneously with the IR measurements [2], Ohishi et al. [4] observed the microwave spectrum of PS and derived from a combined analysis of the IR and MW data a reliable set of ground state molecular parameters. For the $^2\Pi_{1/2}$ and $^2\Pi_{3/2}$ state the authors [4] measured 77 lines with values of $J \leq 16.5$ below 293 GHz with a source-modulated millimeter-wave spectrometer.

In the present paper we extend the two rotational series of the $^2\Pi_{1/2}$ and $^2\Pi_{3/2}$ states into the terahertz region to derive from this larger data basis an accurate set of molecular parameters for PS, but also to gain more insight into deviations from the idealized Hund's coupling case (a) for higher rotational states. As a consequence of the relatively high nuclear masses, the spin $\boldsymbol{S}$ and the electronic angular momentum $\boldsymbol{L}$ are strongly coupled to the internuclear axis, and therefore PS proves to be a typical Hund's case (a) molecule. In addition, these measurements on PS should also partly be seen as an effort to investigate the sub-mm-wave spectra of other phosphorus containing molecules, some of them with potential astrophysical significance, such as PH and CP.

In 1987 Turner and Bally [5] and Ziurys [6] detected the first phosphorus compound in interstellar space: the PN radical was discovered in Orion KL, Sgr B2, and W51. They found that the relative abundance of PN was 10^2 - 10^4 times larger than that expected from gas-phase P chemistry (Thorne et al. 1984 [7], Allen 1973 [8]). Hence it seems probable to discover other phosphorus containing molecules, which would be desirable for understanding the phosphorus chemistry in interstellar space. However, the search for PS in interstellar and circumstellar sources between 97.5 and 98 GHz using the 45 m telescope of the Nobeyama Radio Observatory by Ohishi et al. [4] remained negative.

Reprint requests to Prof. G. Winnewisser; Fax: +49 221 470 5162, E-mail: winnewisser@ph1.uni-koeln.de.

0932–0784 / 99 / 0200–0137 $ 06.00

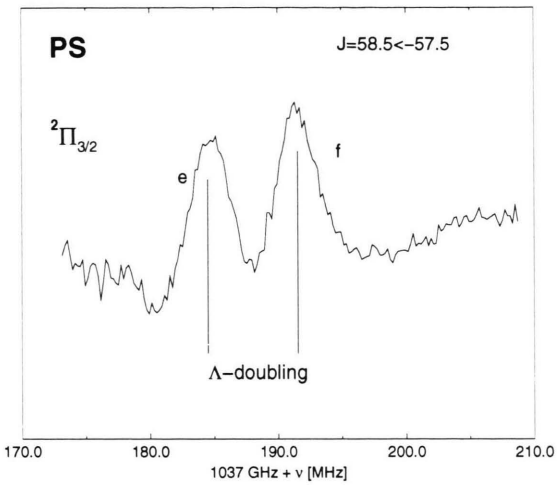

Fig. 1. Sample spectrum of the PS radical in the $^2\Pi_{3/2}$ state at 1.03 THz.

II. Experimental

The Cologne terahertz spectrometer has been described in some detail in [9]. For the present measurements we used two high-frequency and broadband tunable backward wave oscillators (BWOs) as radiation sources (frequency range: 880 - 1100 GHz, output power: $\simeq$ 0.5 mW and 530 - 710 GHz, 2 mW supplied from the ISTOK company). These BWOs were digitally frequency and phase locked to the higher harmonics of a 78 - 118 GHz local oscillator supplied by the KVARZ company. The BWO radiation was frequency-modulated by a double step function of 7 kHz and detected by a magnetically tuned hot electron InSb bolometer. For the detection of very weak lines of paramagnetic species, the Zeeman effect can be advantageously used instead of the commonly employed source modulation technique (see e. g. [10]). However, in the present case the Zeeman modulation did not work out, since the J-values of the affected transitions were too high to be modulated by the applied magnetic field of about 6 Gauss. The PS radical was produced in a dc glow-discharge of $PSCl_3$ in a 2 m long free space absorption cell. We started the measurements by discharching a ($PSCl_3$, Ar) mixture and cooling the absorption cell down to -30°C, as has been done by Ohishi et al. (1988) [4]. However during the measurements we found the PS signal optimal by omitting the cooling of the cell. The best conditions for the PS production were partial pressures of 80 μbar Ar, 3 μbar $PSCl_3$, and 320 mA discharge current.

For well-isolated and strong lines, the measurement accuracy of our spectrometer in the Doppler-limited mode is better than ±5 kHz [11]. Besides, this measurement accuracy can be increased to ±500 Hz in cases where sub-Doppler measurements are possible [12]. The PS spectra have been measured with less accuracy because of a variety of reasons such as partial blending for nearly all hyperfine components of PS, baseline problems, and the rather low production rate of the PS molecule. The measurement accuracy is estimated to be typically 80 kHz for the stronger lines and 200 kHz for the weaker ones. Sample spectra of the resolved Λ-doublets of $J = 58.5 \leftarrow 57.5$ in $^2\Pi_{3/2}$

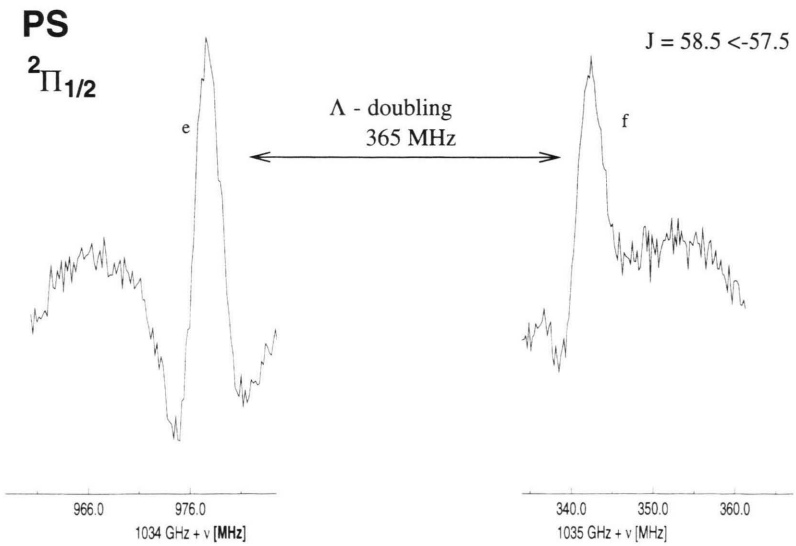

Fig. 2. Sample spectrum of the PS radical in the $^2\Pi_{1/2}$ state at 1.03 THz.

Table 1. Observed Rotational Transitions of PS (in MHz).

J	←	J	Ω	Parity	ν_{obs}	O – C
30.5		29.5	0.5	e	541263.322	0.020
30.5		29.5	0.5	f	541633.835	0.052
30.5		29.5	1.5	e	542524.153	–0.200
30.5		29.5	1.5	f	542526.356	–0.165
31.5		30.5	0.5	e	558970.835	0.019
31.5		30.5	0.5	f	559341.266	0.000
31.5		30.5	1.5	e	560267.334	0.575
31.5		30.5	1.5	f	560269.833	0.977
32.5		31.5	0.5	e	576673.503	–0.550
32.5		31.5	0.5	f	577044.384	0.090
33.5		32.5	0.5	e	594372.770	–0.007
33.5		32.5	1.5	e	595737.540	–0.283
33.5		32.5	1.5	f	595740.082	–0.111
34.5		33.5	0.5	e	612066.883	0.013
34.5		33.5	0.5	f	612436.727	–0.010
34.5		33.5	1.5	e	613466.085	–0.320
34.5		33.5	1.5	f	613468.836	–0.081
35.5		34.5	0.5	e	629756.218	0.018
35.5		34.5	0.5	f	630125.885	0.008
35.5		34.5	1.5	e	631189.865	–0.301
35.5		34.5	1.5	f	631192.755	–0.070
36.5		35.5	0.5	e	647440.671	0.041
36.5		35.5	0.5	f	647810.220	0.050
36.5		35.5	1.5	e	648908.750	–0.217
37.5		36.5	0.5	e	665120.035	0.016
37.5		36.5	0.5	f	665489.314	0.012
37.5		36.5	1.5	e	666622.456	–0.213
37.5		36.5	1.5	f	666625.517	–0.116
38.5		37.5	0.5	e	682794.226	–0.002
38.5		37.5	0.5	f	683163.334	0.024
38.5		37.5	1.5	e	684330.917	–0.214
38.5		37.5	1.5	f	684334.085	–0.167
39.5		38.5	0.5	e	700463.147	0.020
39.5		38.5	0.5	f	700832.018	0.020
39.5		38.5	1.5	e	702034.107	–0.106
39.5		38.5	1.5	f	702037.493	–0.005
40.5		39.5	0.5	e	718126.543	–0.025
40.5		39.5	0.5	f	718495.329	0.103
51.5		50.5	0.5	f	912391.345	0.476
51.5		50.5	1.5	e	914001.880	1.184
51.5		50.5	1.5	f	914007.625	0.296
52.5		51.5	0.5	e	929612.604	0.547
52.5		51.5	0.5	f	929977.636	–0.157
52.5		51.5	1.5	e	931620.904	–0.214
52.5		51.5	1.5	f	931626.319	–0.549
53.5		52.5	0.5	e	947191.684	–0.314
53.5		52.5	0.5	f	947557.239	–0.222
53.5		52.5	1.5	e	949234.914	0.712
53.5		52.5	1.5	f	949240.077	–0.092
54.5		53.5	0.5	e	964764.425	–0.120
54.5		53.5	0.5	f	965129.733	0.003
54.5		53.5	1.5	e	966839.557	–0.252
54.5		53.5	1.5	f	966845.678	–0.317
55.5		54.5	0.5	e	982329.089	–0.473
55.5		54.5	0.5	f	982694.356	–0.107
56.5		55.5	0.5	f	1000251.588	0.066
56.5		55.5	1.5	e	1002027.900	–0.128
56.5		55.5	1.5	f	1002034.916	0.249
57.5		56.5	0.5	e	1017436.912	0.465
57.5		56.5	0.5	f	1017800.957	0.189
57.5		56.5	1.5	e	1019609.692	–0.669
57.5		56.5	1.5	f	1019616.748	–0.483
58.5		57.5	0.5	e	1034977.812	–0.226
58.5		57.5	0.5	f	1035342.508	0.445
58.5		57.5	1.5	e	1037184.760	0.112
58.5		57.5	1.5	f	1037191.532	–0.228
59.5		58.5	0.5	e	1052511.540	–0.004
59.5		58.5	0.5	f	1052874.806	–0.460
59.5		58.5	1.5	e	1054750.767	–0.007
59.5		58.5	1.5	f	1054758.984	0.867
60.5		59.5	0.5	e	1070036.970	0.145
60.5		59.5	0.5	f	1070400.444	0.202

Note: Hyperfine splitted components due to $\Delta F = \pm 1$ collapse in the Doppler-width. Values give center frequencies.

and $^2\Pi_{1/2}$ are shown in Figs. 1 and 2. The integration time was about 2 minutes for these measurements.

III. Results and Discussion

We measured 77 lines of PS in the frequency regions between 541 – 718 and 912 – 1070 GHz, which are listed in Table 1 and 2. These spectra were fitted to an effective Hamiltonian of the form

$$\hat{H}_{eff} = \hat{H}_{SO} + \hat{H}_{SR} + \hat{H}_{Rot} + \hat{H}_{CD} + \hat{H}_{\Lambda D} + \hat{H}_{HFS}, \quad (1)$$

where the subscripts SO, SR, Rot, CD, ΛD, and HFS refer to spin-orbit, spin-rotation, rotational motion, centrifugal distortion, Λ-type doubling, and hyperfine contributions, respectively. The spectroscopic constants governing these interactions are A (spin-orbit), γ and D_γ (spin-rotation), B (rotation), D and H (centrifugal distortion), p, q, D_p (Λ-type doubling), and a, b, c, d, and C_I (hyperfine).

Table 2. Observed Rotational Transitions of PS with $\Delta F = 0$ (in MHz).

J	F	←	J	F	Ω	Parity	ν_{obs}	O – C
32.5	32.0		31.5	32.0	1.5	f	577996.637	0.166
33.5	33.0		32.5	33.0	0.5	f	594383.441	0.017
33.5	33.0		32.5	33.0	0.5	e	594698.935	–0.114
34.5	34.0		33.5	34.0	0.5	e	612392.465	–0.660
38.5	38.0		37.5	38.0	0.5	e	683120.462	0.174

The Hamiltonian was evaluated in a parity basis

$$|\, n^2\Pi_{|\Omega|} v J \pm\rangle = \frac{1}{\sqrt{2}} \left\{ |\, nvJ\Omega S\Lambda\Sigma\rangle \pm (-)^{J-S} |\, nvJ(-\Omega)S(-\Lambda)(-\Sigma)\rangle \right\}, \quad (2)$$

representing Hund's case (a) [15]. For the hyperfine analysis, the basis was extended to include the total angular momentum quantum number F, where

$$\boldsymbol{F} = \boldsymbol{I} + \boldsymbol{J}; \quad (3)$$

and I = 1/2 or depending on the phosphorus atom. In the extended basis, the Hamiltonian can be represented by the 2×2 matrix

$$\begin{pmatrix} \langle {}^2\Pi_{\frac{1}{2}} J' \tfrac{1}{2} F \pm |\, \hat{H}_{\text{eff}} |\, {}^2\Pi_{\frac{1}{2}} J \tfrac{1}{2} F \pm\rangle & \langle {}^2\Pi_{\frac{3}{2}} J' \tfrac{1}{2} F \pm |\, \hat{H}_{\text{eff}} |\, {}^2\Pi_{\frac{1}{2}} J \tfrac{1}{2} F \pm\rangle \\ \langle {}^2\Pi_{\frac{1}{2}} J' \tfrac{1}{2} F \pm |\, \hat{H}_{\text{eff}} |\, {}^2\Pi_{\frac{3}{2}} J \tfrac{1}{2} F \pm\rangle & \langle {}^2\Pi_{\frac{3}{2}} J' \tfrac{1}{2} F \pm |\, \hat{H}_{\text{eff}} |\, {}^2\Pi_{\frac{3}{2}} J \tfrac{1}{2} F \pm\rangle \end{pmatrix}$$

where, for the treatment of PS, the nuclear spin I has been set equal to 1/2. In the following the Hamiltonian will be discussed due to the order of the energy contributions of the individual terms of $\hat{H}_{\text{eff}}$ in (1). For reasons of completeness we refer to the explicit Hamiltonian matrix elements.

III.1. Fine Structure

The fine structure is characterized by the electron spin-orbit- and electron spin-rotation-interaction, where the spin-orbit coupling dominates the splitting. The ground state of PS is a regular $^2\Pi$ state, so that the $^2\Pi_{1/2}$ substate is the energetically lower one. The $^2\Pi_{3/2}$ substate lies nearly 320 cm^{-1} higher and, in the interstellar medium, it will only be populated in high temperature sources. Because of the relatively high nuclear masses of each atom, phosphorus and sulphur, the axial electromagnetic field along the quantization

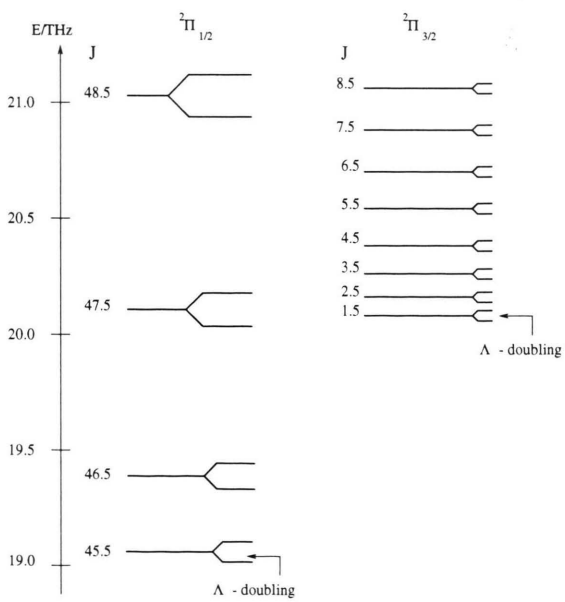

Fig. 3. Section of the energy level diagram of PS.

a-axis is rather strong and therefore leads to a large coupling between the spin $\boldsymbol{S}$ and the electronic angular momentum $\boldsymbol{L}$. This is the reason for the high energy splitting between the two electronic states (see Figure 3). The $^2\Pi_{1/2}$ and $^2\Pi_{3/2}$ arise from the coupling of $\boldsymbol{S}$ and $\boldsymbol{L}$ to form the resultant projection on the *a*-axis $\Omega = \Lambda + \Sigma = \frac{3}{2}$ and $\Omega = \Lambda - \Sigma = \frac{1}{2}$. As a typical property for Hund's case (a) wave functions the projections Λ and Σ on the internuclear axis and therefore Ω are good quantum numbers. For PS, the large energy splitting between the two states $^2\Pi_{3/2}$ and $^2\Pi_{1/2}$, causes the observable transitions corresponding to $\Delta\Omega = \pm 1$ to lie in the FIR, i. e. neither in the submm- nor in the terahertz-region. Nevertheless the value for the fine structure constant A of about 9.6 THz [3] can be used to analyse the pure rotational transitions, since the explicit matrix elements of $\hat{H}_{SO}$ are independent of the rotational quantum number J:

$$\hat{H}_{\text{FS}} = \hat{H}_{\text{SO}} + \hat{H}_{\text{SR}} \quad (4)$$

$$= \frac{1}{2} A \begin{pmatrix} -1 & 0 \\ 0 & 1 \end{pmatrix} + \gamma \begin{pmatrix} -1 & \frac{1}{2}\sqrt{J^2 + J - \frac{3}{4}} \\ \frac{1}{2}\sqrt{J^2 + J - \frac{3}{4}} & 0 \end{pmatrix}.$$

The necessity to take the spin-rotation interaction γ into account for the fit is due to the strong correlation of the matrix elements of γ with those of the Λ-doubling parameter

$$p^* = 2 \sum_{\Pi\text{-states}} \frac{\langle \Pi \mid AL_+ \mid \Sigma^{\pm}\rangle \langle \Pi \mid BL_+ \mid \Sigma^{\pm}\rangle}{E^{\Pi} - E^{\Sigma}}$$

which is independent of the parity function "±". Using perturbation theory, it can be shown that this term

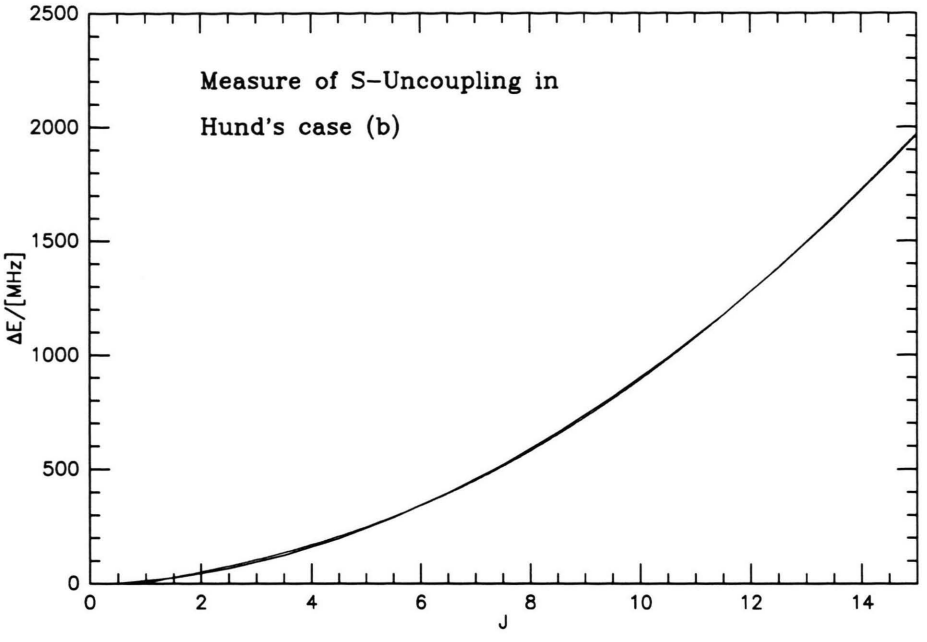

Fig. 4. ***S***-uncoupling in PS is plotted vs. J.

becomes dependent on "±" in the case of neighbouring electronic states and then affects the Λ-doubling. In this case, γ does not represent a contribution to the fine structure, but is instead a manifestation of an additional Λ-doubling contribution between the $^2\Pi$ and the $^2\Sigma$ states.

III.2. Rotational Spectra

The observed pure rotational lines of PS are divided into two sets of transitions arising from the $^2\Pi_{3/2}$ and $^2\Pi_{1/2}$ states. In each fine structure term the typical rotational ladder corresponding to $B \cdot N(N+1)$ of Hund's case (b) can be recognized, now determined by the rotational quantum number $J = N \pm S$ (see Fig. 3). However, the rotational part of the Hamiltonian of the PS radical can be represented by the expression

$$H_{rot} = B \cdot \{J^2 - J_z^2 + S^2 - S_z^2 + \underbrace{(L_+S_- + L_-S_+)}_{\text{Spin-Orbit}} - \underbrace{(J_-S_+ + J_+S_-)}_{\text{Spin-Rot}} - \underbrace{(J_+L_- + J_-L_+)}_{\Lambda\text{-Doubling}}\}, \quad (5)$$

corresponding to the origin vector coupling of a Hund's case (a) molecule. Contrary to Hund's case (b) there is no possibility in case (a) to give a formula for the pure rotational part separately from fine-structure and Λ-doubling contributions. The matrix representation therefore results in

$$\hat{H}_{\text{rot}} = B \begin{pmatrix} J^2 + J + \frac{1}{4} & -\sqrt{J^2 + J - \frac{3}{4}} \\ -\sqrt{J^2 + J - \frac{3}{4}} & J^2 + J - \frac{7}{4} \end{pmatrix}, \quad (6)$$

containing on- and off-diagonal elements in the case (a) parity basis (2). n the case of rotation, off-diagonal elements represent an admixture of Hund's case (b) wave function and lead to the spin-uncoupling from the molecular axis. To determine the size of the ***S***-uncoupling as a function of J with the Hund's case (a) parity basis, we calculated rotational-spin-orbit energies with and without off-diagonal elements and took the difference ΔE between them as a measure of the ***S***-uncoupling in Hund's case (b). This mathematical procedure was developed by Klisch et al. [13]. In Fig. 4 ΔE, plotted for PS, shows an approximative quadratic dependence on J and ranges in size up to $\approx$ 1.9 GHz for $J = 14.5$. A comparison between the ***S***-uncoupling of PS with that of NO – both have $X^2\Pi$-symmetry – shows that the size of the spin-uncoupling of PS is by a factor $\approx$ 70 smaller than for NO, which for higher rotational states is characterized by an intermediate state between Hund's cases (a) and

Table 3. Molecular constants of PS in the electronic and vibrational ground states $^2\Pi_{1/2}$ and $^2\Pi_{3/2}$ (in MHz).

B	8895.7953(18)
D	0.00578458(44)
H	-0.000000000438(57)*
A	321.93†
γ	-699.8(15)*
D_γ	0.00227(28)*
p	372.483(30)
D_p	-0.000174(25)*
q	0.191(12)*
a	516.9(27)*
b	288.2(56)
c	–444.4(52)*
d	686.22(43)
C_I	–0.0349(53)*

(The values in parentheses are the uncertainties in units of the last digits). * Determined for the first time; † in cm^{-1}, fixed, taken from Jenouvrier and Pascat (1978).

(b) (see also Fig. 4 in [13]). Light molecular species, as the hydrides PH [14], SH [15], and NH [16], exhibit much stronger ***S***-uncoupling because of their larger rotational constants. In order to calculate accurate spin-uncoupling energies, a highly precise value for the pure rotational parameter B is required. As a result of our measurements we obtained very accurate values for the rotational parameter B and the centrifugal distortion parameter D (see Table 3). Futhermore, the sextic centrifugal distortion constant H was determined for the first time. It is worth noting that in a pure Hund's case (a) coupling scheme, ***L*** and ***S*** are separately decoupled along the internuclear axis. In PS for lower rotational states, the electronic spin ***S*** is coupled to the molecular axis, as in pure case (a). For higher rotational states, however, ***S*** slowly uncouples from the molecular axis and eventually couples instead to the angular momentum $\boldsymbol{N} = \boldsymbol{\Lambda} + \boldsymbol{R}$, where ***R*** is the end-over-end angular momentum of the nuclear frame and $\boldsymbol{\Lambda}$ is the electronic orbital angular momentum along the nuclear axis, as in pure Hund's case (b). This spin uncoupling leads to a change in the effective rotational constants B_{eff} and thus to characteristic shifts involving the two appropriate energy level stacks consisting of the rotational energy levels of the $X^2\Pi_{1/2}$ and $X^2\Pi_{3/2}$ electronic states. For the $X^2\Pi_{1/2}$ state, the effective rotational constant is [14]

$$B_{\text{eff}} = B_v\left(1 - \frac{B_v}{\Lambda A} + \ldots\right) = 8887.5831\,(18)\,\text{MHz}, \quad (7)$$

whereas for the $X^2\Pi_{3/2}$ state, the effective rotational constant is

$$B_{\text{eff}} = B_v\left(1 + \frac{B_v}{\Lambda A} + \ldots\right) = 8903.9984\,(18)\,\text{MHz}, \quad (8)$$

where the positive value of Λ (=1) is chosen. The frequency shift between the two fine structure terms amounts only to $\approx$ 16 MHz for the PS molecule. This attributes, together with the small spin-uncoupling behaviour to the well practicable Hund's case (a) wave function (2). For NO a value of $\approx$ 260 MHz is found for the frequency shift.

III.3. Λ-Doubling

The electronic angular momentum leads to a degenerated state of J, which in the classical picture, is due to the two different orientations of the electron's motion around the nuclei. The molecular end-over-end rotation, or more precisely the interaction between the electronic angular momentum ***L*** and the rotation ***R***, removes the degeneracy and splits each rotational-fine structure term into two states with different parity. The Λ-doubling energies are in general smaller than the rotational or the fine structure energies. For the NO radical the uncoupling of ***L*** from the internuclear axis has the effect of making the molecule intermediate between Hund's case (a) and (d), in which ***L*** couples to ***R***. For PS this effect is less important; as shown for the ***S***-un_coupling. In general the Λ-doubling splitting is larger for the $^2\Pi_{1/2}$ state than for the the $^2\Pi_{3/2}$ state, which can be understood from the matrix elements:

$$(\hat{H}_{\Lambda D}) = \mp\{p + D_p\,J(J+1)\}\begin{pmatrix} \frac{1}{2}(J+\frac{1}{2}) & 0 \\ 0 & 0 \end{pmatrix} \quad (9)$$

$$\mp\{q + D_q J(J+1)\}\begin{pmatrix} J+\frac{1}{2} & -\frac{1}{2}(J+\frac{1}{2})\sqrt{X} \\ -\frac{1}{2}(J+\frac{1}{2})\sqrt{X} & 0 \end{pmatrix},$$

where $X = J(J+1) - 3/4$ and $\pm$ refers to the parity function.

The splitting of the $^2\Pi_{\frac{1}{2}}$ state is determined by the Λ-type doubling parameters p and q, while the contributions refering to the $^2\Pi_{3/2}$ state are only dependent on the off-diagonal elements in q.

The analysis of Λ-type doubling in terms of a 2×2 matrix is a simplification of the actual situation, in which matrix elements between the Ω components of the $^2\Pi$ state and all $^2\Sigma$ states cause the effect. These matrix elements, connecting states of different

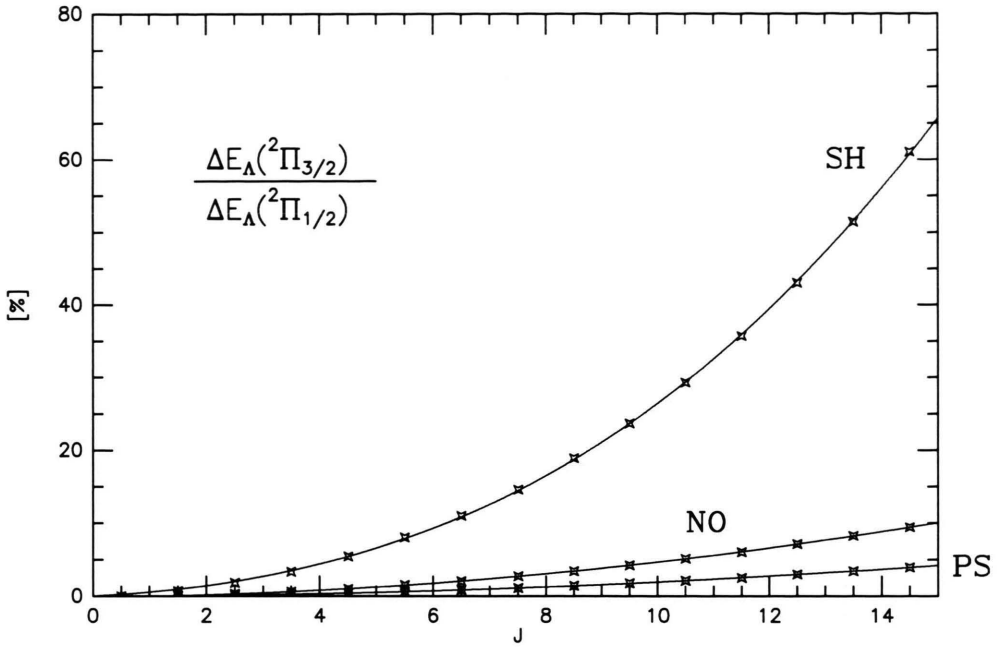

Fig. 5. Ratio of the Λ-type doubling in the $^2\Pi_{3/2}$ state to that in the $^2\Pi_{1/2}$ state plotted as a function of J for the radicals NO, SH, and PS.

Λ ($\Lambda = -1, 0, +1$), have the effect of causing the so-called $\boldsymbol{L}$-uncoupling from the internuclear axis. Eventually, as J increases, $\boldsymbol{L}$ is more profitably coupled to the end-over-end rotation $\boldsymbol{R}$ of the molecule, a situation known as Hund's case (d). Since it is difficult to isolate perturbing $^2\Sigma$ states, a perturbation treatment first presented by van Vleck [18] is normally used. The $(\hat{H}_{\Lambda D})$ matrix shown above is the second-order result. The off-diagonal matrix elements of $(\hat{H}_{\Lambda D})$ are zero for molecules represented exactly by the parity basis of (2). Indeed, this holds for no molecule, since it would require a rotational constant of zero. When off-diagonal elements of $(\hat{H}_{\Lambda D})$ are included, the electron spin $\boldsymbol{S}$, which is coupled to the orbital field of $\boldsymbol{L}$ in Hund's case (a) representation, will show a slight uncoupling due to admixture of Hund's case (d) in addition to its major uncoupling due to admixture of Hund's case (b). It can be stated in other words that while the linear Λ-type doubling in the $^2\Pi_{1/2}$ state is a pure measure of $\boldsymbol{L}$-uncoupling, the Λ-type doubling in the $^2\Pi_{3/2}$ state is caused by a combination of $\boldsymbol{L}$-uncoupling and $\boldsymbol{S}$-uncoupling.

The ratio of the energetically split rotational terms of the $^2\Pi_{3/2}$ to the $^2\Pi_{1/2}$ fine structure term provides a qualitative measure of the joint effect of $\boldsymbol{L}$-uncoupling and $\boldsymbol{S}$-uncoupling compared with the pure uncoupling of $\boldsymbol{L}$. This relation was calculated by first using the off-diagonal elements in (9), which represent the nonlinear contribution of the Λ-doubling causing $(\boldsymbol{L} + \boldsymbol{S})$-uncoupling, and then by omitting the off-diagonal elements, yielding the pure $\boldsymbol{L}$-uncoupling leading to Hund's case (d). In Fig. 5, these ratios are shown for the radicals NO, SH, and PS, all of which are of $^2\Pi$ symmetry. For the PS molecule the ratio is extremely small so that the points are pictured on a scale enlarged by a factor of 50. Based on (9), one expects the ratio to go as the square of the ratio of the rotational constant to the fine structure constant multiplied by a factor roughly quadratic in J, which results from algebraic diagonalization [17, 19, 20]. Thus, light radicals with large rotational constants will show deviations from pure case (a) at lower levels of J. For NO, the ratio of the rotational constant B to the fine structure constant A is roughly 0.01, so that even for J as large as 14.5, the ratio of the Λ-type doubling in the $^2\Pi_{3/2}$ substate to the Λ-type doubling in the $^2\Pi_{1/2}$ substate is still only 0.1. For PS, the ratio is $B/A = 0.0009$, and this radical approximates case (a) almost exactly, such that the analogous ratio is 0.002 at $J = 14.5$. For SH [16, 21] the ratio is much

larger, as pictured in Fig. 4, since $B/A = 0.025$. The ratio B/A corresponds to the often quoted formula $2BJ \ll |\Lambda A|$ and is conform with the explicit matrix formalism of the symmetric wave function. Effects of transitions between the Hund's cases (see Klisch et al. [13]) are compensated for off-diagonal elements.

III.4. Hyperfine Structure

The hyperfine splitting is dominated by the magnetic interactions between the nuclear spin $\boldsymbol{I}$ and the electronic orbital angular momentum $\boldsymbol{L}$ and spin $\boldsymbol{S}$. These interactions exhibit a reverse behaviour from the Λ-doubling, in that the splittings are more pronounced in the $^2\Pi_{3/2}$ state.

The basis used for the hyperfine coupling corresponds to Hund's case (a_β), in which the nuclear spin $\boldsymbol{I}$ couples to $\boldsymbol{J}$ to form a resultant vector $\boldsymbol{F}$.

The diagonal hyperfine matrix elements for the $I = 1/2$ case in this basis used for the numerical fit are given by Brown [22] and Meerts [23]:

$$\begin{aligned}\langle {}^2\Pi_{\frac{1}{2}} J' \frac{1}{2} F\pm \mid \hat{H}_{\mathrm{Hfs}} \mid {}^2\Pi_{\frac{1}{2}} J \frac{1}{2} F\pm\rangle \\ = G(I,J,J',F)\Big\{(-)^{J'-\frac{1}{2}}\begin{pmatrix} J' & 1 & J \\ -\frac{1}{2} & 0 & \frac{1}{2}\end{pmatrix}\left[a - \frac{b+c}{2}\right] \\ \pm(-)^{J-\frac{1}{2}}\begin{pmatrix} J' & 1 & J \\ \frac{1}{2} & -1 & \frac{1}{2}\end{pmatrix}\frac{d}{\sqrt{2}} \\ + 2\delta_{J,J'}(-)^{J'-\frac{1}{2}}\begin{pmatrix} J' & 1 & J \\ -\frac{1}{2} & 0 & \frac{1}{2}\end{pmatrix} X\, C_I\Big\},\end{aligned} \tag{10}$$

$$\begin{aligned}\langle {}^2\Pi_{\frac{3}{2}} J' \frac{1}{2} F\pm \mid \hat{H}_{\mathrm{Hfs}} \mid {}^2\Pi_{\frac{3}{2}} J \frac{1}{2} F\pm\rangle \\ = G(I,J,J',F)\,(-)^{J'-\frac{3}{2}}\begin{pmatrix} J' & 1 & J \\ -\frac{3}{2} & 0 & \frac{3}{2}\end{pmatrix} \\ \cdot\left[a + \frac{b+c}{2} + \delta_{J,J'}\frac{2}{3} X\, C_I\right],\end{aligned} \tag{11}$$

where

$$\begin{aligned}G(I,J,J',F) = (-)^{I+J'+F} \\ \cdot\sqrt{I(I+1)(2I+1)(2J+1)(2J'+1)}\begin{Bmatrix} F & J' & I \\ 1 & I & J\end{Bmatrix}.\end{aligned} \tag{12}$$

The spin-rotation hyperfine interaction parameters C_I and $C_{I'}$ are of second order, as described by Townes and Schawlow [20], who reduce the effect to a perturbation caused by excited states with $\Delta\Lambda = \pm 1$; viz.

$$C_I \propto \sum \frac{\langle \Pi \mid r^{-3} L_+ \mid \Sigma\rangle\langle \Pi \mid B L_+ \mid \Sigma\rangle}{\Delta E}. \tag{13}$$

The nuclear spin-rotation constants typically influence the hyperfine structure of molecules possessing a strong bonding potential. For non-radicals like HC_5N or other carbon chain molecules, the spin-rotation interaction C_I yields one contribution to the hyperfine structure. The magnetic hyperfine parameters a, b, and c cause a larger splitting for the $^2\Pi_{3/2}$ state than for the $^2\Pi_{1/2}$ state as a partial consequence of the different factors $[a - (b+c)/2]$ for $^2\Pi_{1/2}$ and $[a + (b+c)/2]$ for $^2\Pi_{3/2}$ in the diagonal matrix elements.

To understand this, one must look at the off-diagonal matrix elements:

$$\begin{aligned}\langle {}^2\Pi_{\frac{1}{2}} J' \frac{1}{2} F\pm \mid \hat{H}_{\mathrm{Hfs}} \mid {}^2\Pi_{\frac{3}{2}} J \frac{1}{2} F\pm\rangle \\ = -G(I,J,J',F)\,(-)^{J'-\frac{3}{2}}\begin{pmatrix} J' & 1 & J \\ -\frac{3}{2} & 1 & \frac{1}{2}\end{pmatrix} \\ \cdot\frac{b \mp \delta_{J,J'}(J+\frac{1}{2})C_I'}{\sqrt{2}}.\end{aligned} \tag{14}$$

In these terms, the magnetic Fermi-contact interaction constant b represents the dominant contributions. Because the parameter b (see Table 3) is rather small, the magnetic hyperfine interaction is dominated by diagonal contributions, but b affects the hyperfine spectrum due to the numerical diagonalization. In particular, the off-diagonal elements of b cause an increase of the hyperfine splitting of the $^2\Pi_{3/2}$ state and, vice versa, a decrease of the splitting of the $^2\Pi_{1/2}$ state. Since the Fermi contact interaction represents the non-vanishing probability of the unpaired electron to be located near the nucleus, molecules with a significantly larger hyperfine splitting in the $^2\Pi_{3/2}$ state than in the $^2\Pi_{1/2}$ state possess a higher probability for the unpaired electron density to be large near the magnetic nucleus.

For most of our measured transitions it was not possible to resolve the hyperfine splittings caused by the P-atom because of their high J values up to 60.5.

For these quantum numbers, the individual components of the $\Delta F = \pm 1$ transitions collapse within the Doppler-width. However, hyperfine transitions with $\Delta F = 0$ move away from the central position but loose intensity. We have observed 5 hfs components corresponding to relative intensities as low as 0.0002, which for the first time allow a determination of the nuclear spin-rotation interaction constant C_I.

IV. Conclusion

The newly measured lines (listed in Tables 1 and 2) yield a set of molecular parameters, whereby the rotational, the Λ-doubling and the hyperfine parameters could be determined precisely. The rotational parameters (see Table 3) agree very well with those of Ohishi et al. (1988) [4]. In addition, the high rotational transitions require the centrifugal distortion parameter H in the fit. Both parameters for the Λ-doubling, p and q and the centrifugal correction term D_p were determined. All parameters of the magnetic dipole hyperfine structure have been determined, whereby a, c and the second order interaction C_I of the nuclear spin rotation were obtained for the first time. These values are somewhat different from those of Ohishi as a consequence of our measured lines with $\Delta F = 0$.

Acknowledgements

This work was supported in part by the Deutsche Forschungsgemeinschaft (DFG) via grant SFB 301 and special funding from the Science Ministry of the Land Nordrhein-Westfalen.

[1] K. Dressler, Helvetica Phys. Acta **28**, 317 (1955a); ———, Helvetica Phys. Acta **28**, 563 (1955b).
[2] K. Kawaguchi, E. Hirota, M. Ohishi, H. Suzuki, S. Takano, S. Yamamoto, and S. Saito, J. Mol. Spectrosc. **130**, 81 (1988).
[3] A. Jenouvrier and B. Pascat, Canad. J. Phys. **56**, 1088 (1978).
[4] M. Ohishi, S. Yamamoto, S. Saito, K. Kawaguchi, H. Suzuki, N. Kaifu, S. Ishikawa, S. Takano, T. Tsuji, and W. Unno, Astrophys. J. **329**, 511 (1988).
[5] B. E. Turner and J. Bally, Astrophys. J. **321**, L75 (1987).
[6] L. M. Ziurys, Astrophys. J. **321**, L81 (1987).
[7] L. R. Thorne, V. G. Anicich, S. S. Prasad, and W. T. Huntress, Astrophys. J. **280**, 139 (1984).
[8] C. W. Allen, Astrophysical Quantities, 3rd ed., Athlone, London 1973.
[9] G. Winnewisser, Vib. Spectrosc. **8**, 241 (1995).
[10] H. Klein, F. Lewen, R. Schieder, J. Stutzki, and G. Winnewisser, Astrophys. J. Lett. **494**, L125 (1998).
[11] S. P. Belov, F. Lewen, Th. Klaus, and G. Winnewisser, J. Mol. Spectrosc. **174**, 606 (1995).
[12] G. Winnewisser, S. P. Belov, Th. Klaus, and R. Schieder, J. Mol. Spectrosc. **184**, 468 (1997).
[13] E. Klisch, S. P. Belov, R. Schieder, G. Winnewisser, and E. Herbst, J. Mol. Phys., Carrington Special Issue, 1 (1998).
[14] E. Klisch, H. Klein, G. Winnewisser, and E. Herbst, Z. Naturforsch. **53a**, 733 (1998).
[15] E. Klisch, Th. Klaus, S. P. Belov, A. Dolgner, R. Schieder, and G. Winnewisser, Astrophys. J. **473**, 1118 (1996).
[16] Th. Klaus, S. Takano, and G. Winnewisser, Astron. Astrophys. **322**, L1 (1997).
[17] W. Gordy and R. L. Cook, Microwave Molecular Spectra, 3rd ed., John Wiley and Sons, New York (1984).
[18] J. H. van Vleck, The Theory of Electric and Magnetic Susceptibilities, Oxford University Press, London 1932.
[19] A. Carrington, Microwave Spectroscopy of Free Radicals, Academic Press, London (1974).
[20] C. H. Townes and A. L. Schawlow, Microwave Spectroscopy, Dover Publications, Inc., New York 1955.
[21] E. Klisch, Th. Klaus, S. P. Belov, G. Winnewisser, and E. Herbst, in "Amazing Light", ed. R. Y. Chiao, Springer-Verlag, New York 1996, p. 355.
[22] J. M. Brown, M. Kaise, C. M. L. Kerr, and D. J. Milton, J. Mol. Phys. **36**, 553 (1978).
[23] W. L. Meerts, J. P. Bekooy, and A. Dymanus, J. Mol. Phys. **37**, 425 (1979).